Efficient calculation of (resonance) Raman spectra and excitation profiles with real-time propagation

Mattiat, Johann ; Luber, Sandra

Abstract: We investigate approaches for the calculation of (resonance) Raman spectra in a real-time time-dependent density functional theory (RT-TDDFT) framework. Several short time approximations to the Kramers, Heisenberg, and Dirac polarizability tensor are examined with regard to the calculation of resonance Raman spectra: One relies on a Placzek type expansion of the electronic polarizability and the other one relies on the excited state gradient method. The first one is shown to be in agreement with an approach based on perturbation theory in the case of a weak -pulse perturbation. The latter is newly applied in a real time propagation framework, enabled by the use of Padé approximants to the Fourier transform which allow for a sufficient resolution in the frequency domain. An analysis of the performance of Padé approximants is given. All approaches were found to be in good agreement for uracil and R-methyloxirane. Moreover it is shown how RT-TDDFT can be used to calculate Raman excitation profiles efficiently.

DOI: https://doi.org/10.1063/1.5051250

Efficient calculation of (resonance) Raman spectra and excitation profiles with real-time propagation

Cite as: J. Chem. Phys. **149**, 174108 (2018); https://doi.org/10.1063/1.5051250
Submitted: 07 August 2018 . Accepted: 11 October 2018 . Published Online: 05 November 2018

Johann Mattiat, and Sandra Luber

Efficient calculation of (resonance) Raman spectra and excitation profiles with real-time propagation

Johann Mattiat and Sandra Luber[a)]
Department of Chemistry, University of Zurich, Winterthurerstrasse 190, Zurich, Switzerland

(Received 7 August 2018; accepted 11 October 2018; published online 5 November 2018)

We investigate approaches for the calculation of (resonance) Raman spectra in a real-time time-dependent density functional theory (RT-TDDFT) framework. Several short time approximations to the Kramers, Heisenberg, and Dirac polarizability tensor are examined with regard to the calculation of resonance Raman spectra: One relies on a Placzek type expansion of the electronic polarizability and the other one relies on the excited state gradient method. The first one is shown to be in agreement with an approach based on perturbation theory in the case of a weak δ-pulse perturbation. The latter is newly applied in a real time propagation framework, enabled by the use of Padé approximants to the Fourier transform which allow for a sufficient resolution in the frequency domain. An analysis of the performance of Padé approximants is given. All approaches were found to be in good agreement for uracil and R-methyloxirane. Moreover it is shown how RT-TDDFT can be used to calculate Raman excitation profiles efficiently. *Published by AIP Publishing.* https://doi.org/10.1063/1.5051250

I. INTRODUCTION

Real time propagation (RTP) techniques for the solution of the time-dependent Schrödinger equation (TDSE) in a time-dependent density functional theory (TDDFT) framework have become a viable alternative to common perturbation theory (PT) approaches, such as Sternheimer's[1] and Casida's[2] approach to TDDFT, for the calculation of spectroscopic properties.[3,4]

One of the advantages of RTP techniques is that they bring about the full spectrum naturally because spectra are connected via a Fourier transform (FT) to the characteristics of the time evolution, whereas PT methods usually cover only a limited frequency range at a time, e.g., for the calculation of excitation energies and oscillator strengths.[5] For details regarding scaling, see, e.g., Ref. 6. This leads to an advantage in cost if many excited states are involved, as an example for the calculation of spectra of dye in solution.[7] Moreover, RTP approaches can give the response beyond the linear response by including electro-magnetic fields non-perturbatively, which makes them computationally simpler compared to perturbative approaches to non-linear response.[8,9]

Beginning with absorption spectra of C_{60},[10] the application of RTP techniques to chemically relevant systems was extended most notably to hyper-polarizabilities,[11] electronic[12] and magnetic[13] dichroism spectra, molecular conductance,[14] charge transfer,[15] X-ray absorption spectroscopy,[16] the inclusion of relativistic effects in four-component DFT,[17] time-resolved pump probe type spectroscopy,[18] and a phase cycling protocol for X-ray spectroscopy.[19]

In this work, the focus will be on the application of real-time (RT) TDDFT to Raman spectroscopy, especially in the resonant case [resonance Raman spectroscopy (RRS)].[20] The enhancement of the Raman signal when the excitation frequency is near an electronic transition of the molecule opened a wide research field. Among many other applications, RRS was used to gain structural information about bio-molecules,[21] monitor reactions on (catalytic) surfaces,[22] and to investigate nano-structures such as graphene[23] and carbon nano-tubes.[24] Recently, RRS has provided valuable insights into mechanisms in the field of photovoltaics,[25] photo-catalysis,[26] and artificial water splitting.[27] Computational approaches for resonance Raman optical activity for chiral molecules have also been presented.[28–30]

Theoretical efforts to calculate resonance Raman spectra can be broadly categorized into two families of approximations to the perturbation theory result of Kramers, Heisenberg,[31] and Dirac[32] (commonly known as the KHD polarizability tensor), which gives an expression for the electric-dipole–electric-dipole polarizability (for sake of brevity in the following referred to as polarizability) in the Born-Oppenheimer (BO) approximation.

The first kind of approximation was developed by Albrecht[33] *et al.* in the 1960s. In their approach, the electric transition dipole moment is expanded into a Taylor series around the equilibrium geometry. In the resonant case, the resulting terms [the first two terms of the expansion are often called A [Franck–Condon (FC)] and B (Herzberg–Teller)[34] terms] involve a computationally expensive sum over vibrational levels.[35]

On the other hand, Lee, Heller *et al.*[36–38] cast the KHD tensor into the time-domain and justified short time approximations (STA) to the resulting wave package dynamics. A very useful result of them is the excited state gradient method (ESGM), which allows us to calculate relative resonance Raman intensities from the gradient of the excited state BO-surfaces at the ground state equilibrium geometry.

a)Electronic mail: sandra.luber@chem.uzh.ch

Jensen *et al.*[39] also used a short-time approximation to the wave packet dynamics in order to derive a PT-TDDFT expression for the electronic polarizability tensor that is applicable to the resonant case by including a finite phenomenological life time of the electronic excited states. Its application to RRS involves a Placzek type expansion[40] of the electronic polarizability tensor around the equilibrium geometry.[36]

Besides calculations of surface-enhanced Raman spectra via RT-TDDFT,[41,42] Thomas *et al.*[43] have applied the calculation of the electronic polarizability in an RT-TDDFT framework to RRS, also by applying a Placzek type expansion. They compared their results to both Jensen's polarizability method and the excited state gradient method[44] in a PT-TDDFT framework finding a good agreement of the resulting RRS spectra.

In this work, Jensen's approach to calculate the electronic polarizability by using PT is shown to be equivalent to the RT approach in the limit of a weak δ-pulse perturbation. Moreover it is demonstrated how the excited state gradient method can be applied in an RTP framework, instead of using PT-TDDFT. This is enabled by using Padé approximants in the context of the Fourier transforms (FTs) required in RTP techniques which allows for shorter simulation times and, most crucially, for higher resolution in the frequency domain.[45]

In order to support the theoretical findings and compare the results to previous studies, two small molecules have been chosen as model systems: uracil and R-methyloxirane.

The paper is structured as follows: In Sec. II, the necessary theoretical background is given. Details about implementation and calculations are given in Sec. III. The results are presented and discussed in Sec. IV, and a conclusion is given in Sec. V.

II. THEORY

A. KHD polarizability tensor

Usually computational approaches for the calculation of Raman scattering cross sections rely on an expression derived by Kramers, Dirac, and Heisenberg, the KHD polarizability tensor, which describes vibrational Raman scattering in the BO approximation [rotational levels are accounted for by an isotropic average (for more information see Ref. 46)]. Here electronic states are denoted as $|e^k\rangle$ and vibrational states that belong to the electronic BO surface k as $|v_k^n\rangle$. Their energies are E_{e^k} and $E_{e^k}^{v^n}$, respectively.

Then the Raman scattering cross section from an initial state $|v_0^i\rangle$ to a final state $|v_0^f\rangle$, both belonging to the electronic ground state $|e^0\rangle$, is proportional to the KHD polarizability tensor $\alpha_{\alpha\beta}^{\mathrm{KHD}}(\omega)$ given by[47]

$$\alpha_{\alpha\beta}^{\mathrm{KHD}}(\omega) = -\sum_{\substack{v_k^n \neq v_0^i, v_0^f \\ e^k \neq e^0}} \left[\frac{\langle v_0^f|\langle e^0|\hat{d}_\alpha|e^k\rangle|v_k^n\rangle\langle v_k^n|\langle e^k|\hat{d}_\beta|e^0\rangle|v_0^i\rangle}{\hbar\omega - (E_{e^k}^{v^n} - E_{e^0}^{v^i}) + i\hbar\Gamma} + \frac{\langle v_0^f|\langle e^0|\hat{d}_\alpha|e^k\rangle|v_k^n\rangle\langle v_k^n|\langle e^k|\hat{d}_\beta|e^0\rangle|v_0^i\rangle}{-\hbar\omega - (E_{e^k}^{v^n} - E_{e^0}^{v^f}) + i\hbar\Gamma} \right]. \quad (1)$$

Here $\hat{d}_\alpha$ denotes the electric dipole moment operator and the Greek subscripts α and β denote Cartesian directions (x, y, z). Γ accounts phenomenologically for the finite life time of excited states. In principle, each excited state $|v_k^n\rangle$ would have a different life time $\Gamma_{v_k^n}$, but in practice an averaged value is taken. The KHD tensor describes a two photon process: The frequencies of the incoming and scattered photons, ω and ω_S, are related via the energy balance $\hbar\omega_S = \hbar\omega - (E_{e^0}^{v^f} - E_{e^0}^{v^i})$ with $\hbar$ being Planck's constant divided by 2π. The first term dominates if the excitation frequency ω is near or on an electronic resonance ($E_{e^0}^{v^i} + \hbar\omega \approx E_{e^k}^{v^n}$). For the sake of brevity, the second term is referred to as a non-resonant term (NRT) in this paragraph.

The Raman scattering cross section $\sigma_{fi,\alpha\beta}$ for spontaneous Raman scattering is related to the absolute value of the KHD polarizability tensor[38] as follows:

$$\sigma_{fi,\alpha\beta}(\omega) = \left|\Sigma_{\alpha\beta}^{\mathrm{KHD}}(\omega)\right|^2 = \left|\alpha_{\alpha\beta}^{\mathrm{KHD}}(\omega)\right|^2. \quad (2)$$

Lee, Heller *et al.*[38,37] cast the KHD polarizability tensor in the time domain using the algebraic identity

$$\frac{i}{\hbar}\int_0^\infty \mathrm{d}t\, e^{-i(a+ib)t} = \frac{1}{\hbar}\frac{1}{(a+ib)} \quad (3)$$

to rewrite Eq. (1) as[48]

$$\alpha_{\alpha\beta}^{\mathrm{KHD}}(\omega) = \frac{i}{\hbar}\int_0^\infty \mathrm{d}t \sum_{\substack{v_k^n \neq v_0^i, v_0^f \\ e^k \neq e^0}} \Big(\langle v_0^f|\langle e^0|\hat{d}_\alpha|e^k\rangle|v_k^n\rangle \times \langle v_k^n|\langle e^k|\hat{d}_\beta|e^0\rangle|v_0^i\rangle e^{\left(i\left(\omega - \omega_{e^k}^{v^n} + \omega_{e^0}^{v^i}\right) - \Gamma\right)t} + \mathrm{NRT}\Big) \quad (4)$$

with $\omega_{e^k}^{v^n} = E_{e^k}^{v^n}/\hbar$. Considering the action of the Hamiltonian for vibrational motion belonging to the BO-surface of excited state $|e^k\rangle$, $\hat{H}_{e^k}$, on the vibrational state $\langle v_k^n|$,

$$\langle v_k^n|e^{-i\hat{H}_{e^k}t/\hbar} = \langle v_k^n|e^{-i\omega_{e^k}^{v^n}t}, \quad (5)$$

and introducing the Raman wave function

$$|\xi_{e^k e^0,\beta}^i(t)\rangle = e^{-i\hat{H}_{e^k}t/\hbar}\langle e^k|\hat{d}_\beta|e^0\rangle|v_0^i\rangle \quad (6)$$

allows us to write Eq. (4) as

$$\alpha_{\alpha\beta}^{\mathrm{KHD}}(\omega) = \frac{i}{\hbar}\int_0^\infty \mathrm{d}t \sum_{\substack{v_k^n \neq v_0^i, v_0^f \\ e^k \neq e^0}} \Big(\langle \xi_{e^0 e^k,\alpha}^f(0)|v_k^n\rangle\langle v_k^n|\xi_{e^k e^0,\beta}^i(t)\rangle \times e^{\left(i\left(\omega + \omega_{e^0}^{v^i}\right) - \Gamma\right)t} + \mathrm{NRT}\Big). \quad (7)$$

Now the closure over the vibrational states $|v_k^n\rangle$ can be carried out

$$\alpha_{\alpha\beta}^{\mathrm{KHD}}(\omega) = \frac{i}{\hbar}\int_0^\infty \mathrm{d}t \sum_{e^k \neq e^0} \Big(\langle \xi_{e^0 e^k,\alpha}^f(0)|\xi_{e^k e^0,\beta}^i(t)\rangle \times e^{\left(i\left(\omega + \omega_{e^0}^{v^i}\right) - \Gamma\right)t} + \mathrm{NRT}\Big). \quad (8)$$

This time-domain expression for the KHD polarizability tensor is equivalent to its frequency-domain counterpart [see Eq. (1)]. Computational efforts for the calculation of Raman

spectra often require approximations to the KHD polarizability tensor, which usually involve a STA of the excited state dynamics in the resonant case. The time domain formulation of the KHD polarizability tensor [Eq. (8)] gives an intuitive interpretation of STAs:[38] Initially $|\xi^{f}_{e^0e^k,\alpha}(0)\rangle$ and $|\xi^{i}_{e^ke^0,\beta}(t)\rangle$ are localized in the Franck–Condon (FC) region and their initial overlap decays rapidly, on a femto second scale. In many cases, recurrences of the $|\xi^{i}_{e^ke^0,\beta}(t)\rangle$ to the FC region do not contribute significantly to the overlap, among other reasons, due to damping and dephasing. As a consequence, it is sufficient to consider the polarizability tensor only near the FC region of the electronic ground state, also for the calculation of resonance Raman spectra.

1. Non-resonant case and Placzek type expansion

In the case of non-resonant Raman spectroscopy (NRS), the KHD tensor can be reduced to the expression derived by Placzek,[40] by replacing the vibronic energies with their electronic counterparts at the equilibrium geometry q_0, $E^{v^n}_{e^k} \approx E_{e^k}$, $E^{v^i}_{e^0} \approx E_{e^0}$, setting $\omega = \omega_S$, and omitting Γ, which allows us to perform the closure over the vibrational states. This leads to the following expression for the non-resonant electronic polarizability $\alpha^{\text{el, NRS}}_{\alpha,\beta}$:[36]

$$\alpha^{\text{el, NRS}}_{\alpha\beta}(\omega,q) = -\sum_{e^k\neq e^0}\left[\frac{\langle e^0|\hat{d}_\alpha|e^k\rangle\langle e^k|\hat{d}_\beta|e^0\rangle}{\hbar\omega-(E_{e^k}-E_{e^0})} + \frac{\langle e^0|\hat{d}_\alpha|e^k\rangle\langle e^k|\hat{d}_\beta|e^0\rangle}{-\hbar\omega-(E_{e^k}-E_{e^0})}\right]. \tag{9}$$

These assumptions are valid for a clear separation of the energy scales of the electronic transitions, the exciting photon energy, and the vibrational levels.[36,46]

The electronic polarizability $\alpha^{\text{el}}_{\alpha\beta}(\omega,q)$ depends parametrically on the nuclear coordinates q. Then the Raman scattering cross section is proportional to

$$\left|\Sigma^{\text{adiabatic}}_{fi,\alpha\beta}(\omega,q)\right|^2 = \left|\langle v^f_0|\alpha^{\text{el}}_{\alpha\beta}(\omega,q)|v^i_0\rangle\right|^2. \tag{10}$$

Placzek expanded the electronic polarizability into a Taylor series around the equilibrium geometry q_0, leading to[40]

$$\Sigma^{\text{adiabatic}}_{fi,\alpha\beta}(\omega,q) = \alpha^{\text{el}}_{\alpha\beta}(\omega,q)\big|_{q=q_0}\langle v^f_0|v^i_0\rangle + \sum_k \frac{\partial\alpha^{\text{el}}_{\alpha\beta}(\omega,q)}{\partial q_k}\Big|_{q=q_0}\langle v^f_0|q_k|v^i_0\rangle + \ldots, \tag{11}$$

where q_k are mass-weighted normal coordinates for normal mode k. In the harmonic approximation, the terms of the Taylor expansion can be assigned to different sorts of spectroscopy[49,50] and the usual selection rules apply: The 0th order term represents Rayleigh scattering and the 1st order term fundamental Raman scattering.

The differential Raman scattering cross section per solid angle Ω for Stokes scattering can then be calculated according to the following formula for a specific normal coordinate q_k, a scattering angle of 90°, and linearly polarized light with the electric field vector perpendicular to the scatter plane:[46]

$$\frac{d\sigma}{d\Omega} = \frac{\pi^2}{\epsilon_0^2}(\tilde{\nu}_{\text{in}}-\tilde{\nu}_{q_k})^4\frac{h}{8\pi^2c\tilde{\nu}_{q_k}} \times\frac{45|a_{q_k}|^2+7\gamma^2_{q_k}}{45}\frac{1}{1-\exp(-\frac{hc\tilde{\nu}_{q_k}}{k_BT})}, \tag{12}$$

where $\tilde{\nu}_{in}$ is the wavenumber of the incoming light, $\tilde{\nu}_{q_k}$ is the wavenumber of the normal coordinate q_k, ϵ_0 is the vacuum permittivity, c is the speed of light in vacuum, a_{q_k} is the isotropic derivative,

$$a_{q_k} = \frac{1}{3}\sum_\alpha\left(\frac{\partial\alpha_{\alpha\alpha}}{\partial q_k}\right), \tag{13}$$

and $\gamma^2_{q_k}$ is the anisotropic derivative,

$$\gamma^2_{q_k} = \frac{1}{2}\sum_{\alpha\beta}\left[3\left(\frac{\partial\alpha_{\alpha\beta}}{\partial q_k}\right)\left(\frac{\partial\alpha_{\alpha\beta}}{\partial q_k}\right)-\left(\frac{\partial\alpha_{\alpha\alpha}}{\partial q_k}\right)\left(\frac{\partial\alpha_{\beta\beta}}{\partial q_k}\right)\right]. \tag{14}$$

The derivatives are performed numerically using the scheme given in Refs. 51 and 52.

There has been a long standing effort to enable the use of Placzek's expansion also in the resonant case: Warshel and Dauber[53] suggested a way to evaluate Albrecht's A and B terms directly in the resonant case by introducing a Taylor expansion of the vibronic transition dipole moments. Lee searched for appropriate approximations of the KHD tensor by using the time domain description.[36] In the non-resonant case, Placzek's expansion reproduces Albrecht's A and B terms exactly.[36]

2. Jensen's polarizability method

In order to use a Placzek type treatment of vibration also in the resonant case, Jensen *et al.*[39] derived a semi-classical (SC) expression for the electronic polarizability tensor following Lee's original SC treatment of the KHD tensor.[36] Here the propagation in Eq. (8) is cast into Wigner phase space and the propagator is approximated to first order in t by its classical counterpart. A restriction to the Franck–Condon region leads to the semi-classical Raman scattering cross section $\sigma^{\text{SC}}_{fi,\alpha\beta}(\omega) = \left|\Sigma^{\text{SC}}_{fi,\alpha\beta}(\omega)\right|^2$ [$|\xi^{i}_{e^0e^k,\beta}\rangle$ are the Raman wave functions given in Eq. (6), with the time-dependence made explicit]

$$\Sigma^{\text{SC}}_{fi,\alpha\beta}(\omega) = \frac{i}{\hbar}\int_0^\infty dt\sum_{e^k}\langle\xi^{f}_{e^0e^k,\alpha}|e^{-iE_{e^k}/\hbar t}|\xi^{i}_{e^ke^0,\beta}\rangle e^{i(E_0/\hbar+\omega)t-\hbar\Gamma t} - \frac{i}{\hbar}\int_0^\infty dt\sum_{e^k}\langle\xi^{f}_{e^0e^k,\alpha}|e^{iE_{e^k}/\hbar t}|\xi^{i}_{e^ke^0,\beta}\rangle \times e^{i(-E_0/\hbar+\omega_S)t-\hbar\Gamma t}. \tag{15}$$

Transferring to the frequency domain and assuming $\omega \approx \omega_S$ give for the adiabatic polarizability

$$\Sigma^{\text{SC, adiabatic}}_{fi,\alpha\beta}(\omega,q) = \langle v^i_0|\alpha^{\text{el, SC}}_{\alpha\beta}(\omega,q)|v^f_0\rangle, \tag{16}$$

$$\alpha^{\text{el, SC}}_{\alpha\beta}(\omega,q) = \sum_{e^k\neq e^0}\left[\frac{\langle e^0|\hat{d}_\alpha|e^k\rangle\langle e^k|\hat{d}_\beta|e^0\rangle}{-\hbar\omega+(E_{e^k}-E_{e^0})-i\hbar\Gamma} + \frac{\langle e^0|\hat{d}_\alpha|e^k\rangle\langle e^k|\hat{d}_\beta|e^0\rangle}{\hbar\omega+(E_{e^k}-E_{e^0})+i\hbar\Gamma}\right]. \tag{17}$$

It can be used in a Placzek type expansion to calculate NRS and RRS spectra. The only difference to the non-resonant expression in Eq. (9) is the inclusion of a finite life time Γ of the electronic states.

3. Excited state gradient method

By taking a purely classical propagation scheme for the short time wave packet dynamics in Eq. (8) and assuming a harmonic ground state BO surface, Heller *et al.* derived the following formula for the relative Raman intensities of different vibrational modes:[38]

$$\frac{I^k}{I^{k'}} = \frac{\omega_{k'}}{\omega_k}\left(\frac{V_k}{V_{k'}}\right)^2, \tag{18}$$

where

$$V_k = \frac{\partial E_{\mathrm{ex}}}{\partial q_k}\Big|_{q=q_0}, \tag{19}$$

with the mass-weighted normal coordinate q_k corresponding to the normal mode frequency ω_k and E_{ex} the excitation energy of the electronic transition. This became known as the excited state gradient method (ESGM) and should only be used on and near resonances (i.e., in the Condon approximation).[38] In this paper, we will apply this method in an RT-TDDFT framework as shown in Sec. III. Equations (18) and (19) are applicable in that form if only a single electronic state is contributing to the resonance and should only be used for well separated (i.e., usually low-lying) electronic transitions.[39,54]

B. Linear response theory

In this paragraph, the real-time propagation and the perturbative approach to obtain the electronic polarizability are formulated in the framework of response theory. This presentation of linear response theory is closely following Jensen's book, and we refer for more details to Ref. 55. Two general expressions for the linear response, one in an RTP framework and the other in a PT framework will be derived and applied to the specific case of a light–matter electric-dipole–electric-dipole interaction. The discussion will be restricted to electronic responses, which will later be used for the calculation of Raman spectra according to Placzek's expansion [see Eq. (11)]. In order to simplify notation, electronic states are denoted as $|k\rangle$ and their respective energies as E_k. $\hat{H}_0$ is the unperturbed, time-independent Hamiltonian of the (electronic) system in the BO approximation, giving rise to a complete set of eigenstates $\hat{H}_0|m\rangle = E_m|m\rangle$ and the density operator $\hat{\rho}_0 = \sum_m p_m|m\rangle\langle m|$ with $p_m = |c_m|^2$ denoting the probability amplitude of finding a general superposition $|\Psi\rangle = \sum_m c_m|m\rangle$ in eigen-state $|m\rangle$. $\hat{H}_1$ is a time-dependent perturbation Hamiltonian of the general form,

$$\hat{H}_1(t) = -\hat{A}f(t), \tag{20}$$

e.g., a perturbation due to an electric field in the dipole approximation with $\hat{A} = \hat{d}$ and $f(t) = E(t)$ describing the strength and time dependence of the field.

The density matrix $\hat{\rho}(t)$ of the total Hamiltonian $\hat{H}(t) = \hat{H}_0 + \hat{H}_1(t)$ then becomes time-dependent and the expectation value of an operator $\hat{B}$ at time t can be written as

$$\langle\hat{B}(t)\rangle = \mathrm{Tr}\left[\hat{\rho}(t)\hat{B}\right]. \tag{21}$$

The assumption in linear response theory is that this expectation value changes linearly with $f(t)$. If perturbations at different times are independent of each other, this assumption can be cast into the following formula:

$$\langle\hat{B}(t)\rangle - \langle\hat{B}\rangle = \int_{-\infty}^{t} \mathrm{d}t'\, \Phi_{BA}(t-t')f(t'), \tag{22}$$

where Φ_{BA} is called the (linear) response function (of operator $\hat{B}$ with respect to a perturbation operator $\hat{A}$) and $\langle\hat{B}\rangle = \langle\hat{B}(t\to-\infty)\rangle$ being the expectation value of the unperturbed system. The perturbation is assumed to be turned on adiabatically and $\Phi_{BA}(t-t') = 0$ for $t' > t$ due to causality.

In the frequency domain, the response is expressed by the Laplace transform $\chi_{BA}(\omega)$ of the response function,

$$\chi_{BA}(\omega) = \lim_{\epsilon\to0^+}\int_0^\infty \mathrm{d}t\, \Phi_{BA}(t)e^{i(\omega+i\epsilon)t}. \tag{23}$$

The generalized Fourier transform of the expectation value can then be written as

$$\langle\hat{B}(\omega)\rangle = \lim_{\epsilon\to0^+}\int_{-\infty}^{\infty} \mathrm{d}t\, \left(\langle\hat{B}(t)\rangle - \langle\hat{B}\rangle\right)e^{i\omega t}e^{-\epsilon t}. \tag{24}$$

Using the convolution theorem for FTs, one obtains the following relation for the generalized susceptibility $\chi_{AB}(\omega)$:

$$\langle\hat{B}(\omega)\rangle = \chi_{BA}(\omega)f(\omega). \tag{25}$$

1. Linear response in a real-time framework and real-time polarizability method

In the case of a perturbation by an electric field in the dipole approximation and a measurement of the electric dipole moment $\left(\hat{A} = \hat{d}, \hat{B} = \hat{d}\right)$, the generalized susceptibility $\chi_{dd}(\omega)$ is called polarizability tensor $\alpha_{\alpha\beta}$ and thus given by

$$\alpha_{\alpha\beta}(\omega) = \frac{\langle\hat{d}_\alpha(\omega)\rangle}{E_\beta(\omega)}, \tag{26}$$

where $E_\beta(\omega)$ denotes the FT of the electric field in direction β and $\langle\hat{d}_\alpha(\omega)\rangle$ the FT of the electric dipole moment in direction α

$$\langle\hat{d}_\alpha(\omega)\rangle = \lim_{\epsilon\to0^+}\int_{-\infty}^{\infty} \mathrm{d}t\, \left(\langle\hat{d}_\alpha(t)\rangle - d_{0,\alpha}\right)e^{i\omega t}e^{-\epsilon t}. \tag{27}$$

$d_{0,\alpha}$ denotes the static electric dipole moment of the unperturbed system. In real-time propagation, the expectation value of the time-dependent electric dipole moment is simply expressed in the Schrödinger picture using the electronic wave functions $\Psi(t)$ of the system at time t,

$$\langle\hat{d}_\alpha(t)\rangle = \langle\Psi(t)|\hat{d}_\alpha|\Psi(t)\rangle. \tag{28}$$

Equations (26)–(28) are our working equations for obtaining the frequency dependent electronic polarizability tensor $\alpha_{\alpha\beta}(\omega)$ in an RT-TDDFT framework. A brief summary of RTP in a time-dependent Kohn–Sham framework is given in Appendix B.

If only the linear response of a system under study is required, it can be calculated in RTP methods by applying an initial weak δ-pulse, $E_\alpha(t) = \kappa_\alpha\delta(t)$, yielding the perturbation Hamiltonian

$$\hat{H}_1(t) = -\kappa_\alpha \hat{d}_\alpha \delta(t), \tag{29}$$

where κ_α denotes the field strength in the α-direction. This method is referred to as the RT polarizability method in the remainder of this work, and the resulting electronic polarizability tensor is called $\alpha^{\text{el, RT}}_{\alpha\beta}(\omega)$. The derivatives required for the Raman scattering cross section [see Eq. (11)] are performed numerically. The great advantage of employing an RTP technique is that the whole frequency-dependent polarizability is obtained in one simulation run via the FT in Eq. (27) and allows us to calculate NRS and RRS at once.

The absorption strength function $S(\omega)$ is related to the imaginary part of the electronic polarizability $\alpha^{\text{el, RT}}_{\alpha\beta}(\omega)$ as follows:

$$S(\omega) = \frac{4\pi\omega}{3c}\text{Tr}\left\{\text{Im}(\alpha^{\text{el, RT}}_{\alpha\beta}(\omega))\right\}. \tag{30}$$

2. Linear response in a perturbation theory framework

Instead of explicitly calculating the evolution of perturbed time-dependent wave functions, the linear response can be expressed in terms of unperturbed wave functions and the perturbation Hamiltonian by using time-dependent PT. A derivation of relevant formulae is sketched in Appendix A.

For the specific case of a perturbation by an electric field in the dipole approximation and a measurement of the electric dipole moment $\left(\hat{A} = \hat{d}, \hat{B} = \hat{d}\right)$, the linear response function to first order is

$$\begin{aligned}
K_{d_\alpha d_\beta}(t) &= \frac{i}{\hbar}\text{Tr}\left\{\hat{\rho}_0\left[e^{i\hat{H}_0 t/\hbar}\,\hat{d}_\alpha\, e^{-i\hat{H}_0 t/\hbar}, \hat{d}_\beta\right]\right\} \\
&= \frac{i}{\hbar}\sum_{m,k} p_m \Big[e^{iE_m t/\hbar}\langle m|\hat{d}_\alpha|k\rangle e^{-iE_k t/\hbar}\langle k|\hat{d}_\beta|m\rangle \\
&\quad - \langle m|\hat{d}_\alpha|k\rangle e^{iE_k t/\hbar}\langle k|\hat{d}_\beta|m\rangle e^{-iE_m t/\hbar}\Big] \\
&= \frac{i}{\hbar}\sum_{m,k} p_m \Big[\langle m|\hat{d}_\alpha|k\rangle\langle k|\hat{d}_\beta|m\rangle e^{-i(E_k-E_m)t/\hbar} \\
&\quad - \langle m|\hat{d}_\alpha|k\rangle\langle k|\hat{d}_\beta|m\rangle e^{-i(E_m-E_k)t/\hbar}\Big].
\end{aligned} \tag{31}$$

Starting from the electronic ground state $|m\rangle = |0\rangle$, i.e., $p_0 = 1$, and taking the Laplace transform [Eq. (23)], one arrives to first order in the perturbation at the following expression for the frequency-dependent electric-dipole–electric-dipole susceptibility, which we call $\alpha^{\text{el, PT}}_{\alpha\beta}(\omega)$:

$$\begin{aligned}
\alpha^{\text{el, PT}}_{\alpha\beta}(\omega) &= \lim_{\epsilon\to 0^+}\int_0^\infty \text{d}t\; K_{dd} e^{i(\omega+i\epsilon)t} \\
&= \lim_{\epsilon\to 0^+}\int_0^\infty \text{d}t\; \frac{i}{\hbar}\sum_{k\neq 0}\Big[\langle 0|\hat{d}_\alpha|k\rangle\langle k|\hat{d}_\beta|0\rangle \\
&\quad \times e^{i(\hbar\omega+i\hbar\epsilon-E_k+E_0)t/\hbar} \\
&\quad - \langle 0|\hat{d}_\alpha|k\rangle\langle k|\hat{d}_\beta|0\rangle e^{i(\hbar\omega+i\hbar\epsilon-E_0+E_k)t/\hbar}\Big] \\
&= -\lim_{\epsilon\to 0^+}\sum_{k\neq 0}\left[\frac{\langle 0|\hat{d}_\alpha|k\rangle\langle k|\hat{d}_\beta|0\rangle}{\hbar\omega-(E_k-E_0)+i\hbar\epsilon}\right. \\
&\quad \left. - \frac{\langle 0|\hat{d}_\alpha|k\rangle\langle k|\hat{d}_\beta|0\rangle}{\hbar\omega+(E_k-E_0)+i\hbar\epsilon}\right],
\end{aligned} \tag{32}$$

using the algebraic identity given in Eq. (3). Setting ϵ to a finite small value Γ, this expression is the same as the one derived by Jensen from a SC approximation of the KHD polarizability tensor [see Eq. (17)]. In the regime of validity of perturbation theory, thus the RT polarizability method and the PT polarizability method are expected to yield very similar results. This was indeed observed by Thomas *et al.*[43]

In fact, for a weak δ-pulse perturbation [see Eq. (29)], the RT polarizability method can be shown to correspond to the PT polarizability method as follows: The linear response formula (A6) can be used directly to calculate the time-dependent expectation value of the electric dipole moment to first order, under the assumption that κ_β is sufficiently small

$$\langle\hat{d}_\alpha(t)\rangle - \langle\hat{d}_\alpha\rangle = \int_{-\infty}^{t}\text{d}t'\; K_{\alpha\beta}(t-t')\kappa_\beta\delta(t'). \tag{33}$$

Inserting Eq. (31), starting from the ground state, and integrating out the δ distribution give

$$\begin{aligned}
\langle\hat{d}_\alpha(t)\rangle - \langle\hat{d}_\alpha\rangle &= \frac{i}{\hbar}\kappa_\beta\sum_{k\neq 0}\Big[\langle 0|\hat{d}_\alpha|k\rangle\langle k|\hat{d}_\beta|0\rangle e^{-i(E_k-E_0)t/\hbar} \\
&\quad - \langle 0|\hat{d}_\alpha|k\rangle\langle k|\hat{d}_\beta|0\rangle e^{-i(E_0-E_k)t/\hbar}\Big] \\
&= \frac{2}{\hbar}\kappa_\beta\sum_{k\neq 0}\sin\left(\frac{(E_k-E_0)t}{\hbar}\right)\langle 0|\hat{d}_\alpha|k\rangle\langle k|\hat{d}_\beta|0\rangle.
\end{aligned} \tag{34}$$

Taking the FT according to Eq. (27), identifying ϵ with Γ and dividing by $E_\beta(\omega) = \kappa_\beta$ [Eq. (26)] one arrives at the same expression for the electronic polarizability as the direct calculation of the susceptibility in Eq. (32).

C. Padé approximants and RT excited state gradient method

Instead of using PT-TDDFT for the excited state gradient approximation, as is routinely done,[43,54] the latter can also be performed in an RT-TDDFT framework: In order to do so, a very fine frequency resolution of the Fourier transform [see Eq. (27)] is required, which is usually not achieved by the fast Fourier transform (FFT) algorithm due to computational limits (the resolution is $\propto \frac{1}{\Delta t N_{\text{steps}}}$; i.e., at a time step of $\Delta t = 0.1$ a.u., a resolution of 0.0001 eV would require roughly 30 000 000 steps).

As pointed out by Bruner *et al.*,[45] the application of Padé approximants[56,57] to the Fourier transform may be used in order to achieve sufficient resolution and decrease the required simulation time.

The idea is to write the discrete Fourier transform of the dipole moment $d(t)$ as a polynomial in $z = e^{-i\omega\Delta t}$ as

$$d(\omega) = \sum_{k=0}^{M} d(t_k)e^{-i\omega t_k} = \sum_{k=0}^{M} c_k z^k \equiv d(z), \tag{35}$$

where $c_k = d(t_k)$ is the electric dipole moment at time step $t_k = k\Delta t$. Then it can be approximated by the Padé approximation

$$d(z) = \frac{\sum_{k=0}^{N} a_k z^k}{\sum_{k=0}^{N} b_k z^k}. \tag{36}$$

The coefficients a_k and b_k are found by solving the set of linear equations given by equating the terms in Eq. (36) in powers of z. With these at hand, the Fourier transform can be extrapolated for an arbitrary resolution in the frequency domain. This in turn allows us to determine the peak positions in the absorption spectrum (excited state energies) up to the desired precision and thus, by taking a numerical derivative with respect to normal coordinates, the gradients of the excited state surfaces at the ground state geometry are required for the application of the excited state gradient method [see Eq. (19)].

III. COMPUTATIONAL DETAILS

A. RT polarizability method

The RT-TDDFT runs were performed using the package CP2K.[58,59] In this implementation, the numerical solution of the time-dependent Kohn–Sham (TDKS) [Eq. (B1)] proceeds as follows: The electron density (and therefore the KS-Hamiltonian) is extrapolated in time by the always stable predictor corrector method and then converged self-consistently. The enforced time reversible symmetry (ETRS) and the exponential mid-point (EM) propagator are implemented to propagate the electronic density, among others.[7] For sufficiently small time steps, no significant difference between those two propagators was detectable. For pseudopotential basis sets, ETRS was used and for all electron basis sets EM because the EM propagator appeared to be more stable for the Gaussian and augmented plane wave (GAPW) method.

Gaussian type Goedecker–Teter–Hutter (GTH) pseudopotential basis sets[60] and all electron basis sets from Ahlrichs[61] were used in combination with CP2K's Gaussian and plane wave (GPW) and GAPW methods,[62,63] respectively. Three functionals were investigated: The Perdew-Burke-Ernzerhof (PBE) functional,[64] its hybrid version PBE0,[65,66] and the BP86 functional.[67,68]

The time step in the simulations was chosen to be 0.1 a.u. for the GPW method and 0.05 a.u. for the GAPW method. The smaller time step for the GAPW method is necessary in order to get a sufficient sampling rate in the RTP because the last resolved feature in the full absorption spectrum appears at higher frequencies compared to using GPW with pseudopotentials. The RTP runs were run for a total amount of 5000 a.u. (≈120 fs) simulation time in both cases.

All RT-spectra shown in this work are calculated using Padé approximants to the Fourier transform, if not mentioned otherwise. An assessment of the convergence of the Padé approximants is given in Sec. IV.

The phenomenological damping factor Γ was set to 0.1 eV ≈ 0.0037 a.u. in accordance with the choice in the literature,[28,39,54] if not mentioned otherwise.

In order to obtain the full absorption (Raman) spectrum, a total of 3 ($3 * 2 * N_q$, with N_q being the number of normal modes of interest) runs are necessary, if the differentiation of the polarizability tensor along mass-weighted normal coordinates is carried out numerically using a standard three point differentiation scheme.[69]

The actual protocol used to obtain Raman intensities in the RTP framework can be summarized as follows:

1. A geometry optimization with the chosen basis set and functional was performed.
2. A normal mode analysis on the optimized geometry is carried out in order to obtain the normal mode frequencies and coordinates.
3. Two geometries, one displaced along the positive and one along the negative normal mode coordinates, were generated for every normal mode of interest using a step size of 0.005 bohr. Several tests were performed to confirm that this is a reasonable choice.
4. RTP runs were performed for each of the displaced geometries, and the electric dipole moment was recorded in time. The initial δ-pulse perturbation corresponds to

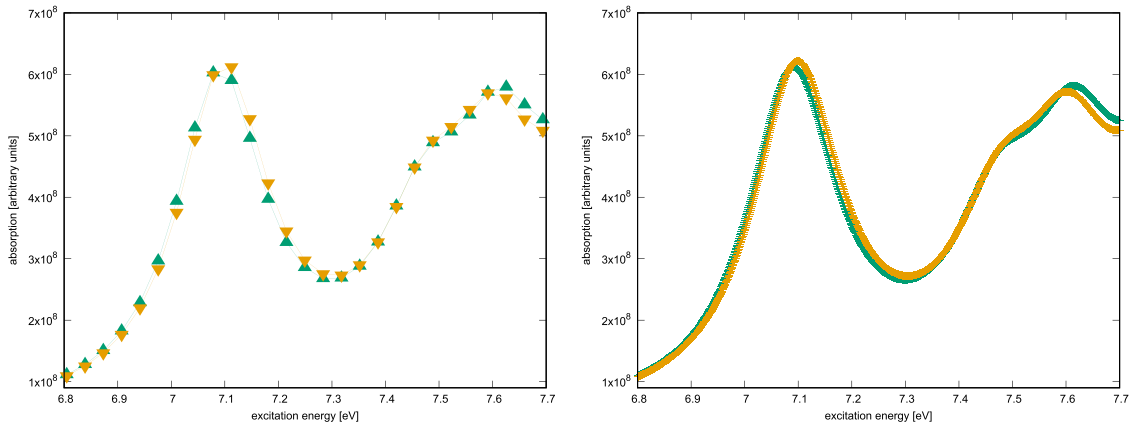

FIG. 1. Comparison between absorption spectra of R-methyloxirane calculated with the FFT algorithm and Padé approximants. In contrast to the FFT, which is only defined at certain points, the Padé approximants extrapolate the FT to an arbitrary resolution. The RTP step size was set to 0.10 a.u. The PBE exchange–correlation functional and the TZV2P-GTH basis set were used. (a) Absorption spectrum calculated using FFT for two geometries slightly displaced along a normal coordinate, one positively (yellow, triangles pointing downwards), one negatively (green, triangles pointing upwards). (b) Absorption spectrum calculated using Padé approximants for two geometries slightly displaced along a normal coordinate, one positively (yellow), one negatively (green).

the multiplication of a phase factor[70] of $e^{i\kappa_\alpha r_\alpha}$ (in atomic units) and was applied to the ground state DFT wave function. The field strength parameter in CP2K was set to 0.001 a.u., resulting in an effective field strength of 2.2166×10^{-4} a.u. for uracil and 2.7708×10^{-4} a.u. for R-methyloxirane. All simulations were carried out using non-periodic boundary conditions.

5. The resulting polarizabilities and its numerical derivatives were evaluated according to Eqs. (12)–(14).

Geometry optimizations, normal mode analysis, and RTP runs were carried out using CP2K; a python suite was created for displacing the geometries, parsing the output of CP2K, and evaluating the electric dipole signals. The python code for performing the Padé approximants was adapted from https://github.com/jjgoings/pade.

B. RT excited state gradient method

For the real-time excited state gradient method (RT-ESGM), the same RTP runs as for the RT polarizability method are used and the same choice of parameters applies. Here the derivatives of the excited state energies with respect to normal coordinates [see Eqs. (18) and (19)] are performed numerically as follows: As mentioned in Sec. II, Padé approximants allow for a sufficient resolution in the frequency domain and therefore to obtain the excitation energies (peak positions) in the absorption spectrum to the desired precision by using a simple minimax search such as the golden section search algorithm.[71] The gradient of a specific normal mode is then obtained by the finite difference scheme for the geometry displaced positively and the geometry displaced negatively along the normal coordinate.

The shift of absorption peaks along a normal mode is illustrated in Fig. 1 for using a conventional FFT on the one hand and Padé approximants on the other hand.

C. PT-TDDFT Raman

In order to compare the RT results with traditional PT-TDDFT, the program Turbomole[72] was used for the calculation of NRS spectra. This implementation is based on analytical derivatives of a polarizability Lagrangian.[73] It is restricted to non-resonant and near-resonance Raman spectra.[74] The TZVP basis set and the PBE and BP86 functionals were used.

IV. RESULTS AND DISCUSSION

The results are discussed in Secs. IV A–IV E: First the convergence of Padé approximants to the FFT algorithm is evaluated. Then absorption spectra calculated with RT-TDDFT and PT-TDDFT, respectively, are discussed for uracil and R-methyloxirane as a validation of the RTP approach. Then NRS spectra obtained by the analytical gradient (PT-TDDFT) method in Turbomole are compared with the NRS spectra from RT-TDDFT in CP2K for the same molecules.

Resonance Raman (RR) spectra obtained with the RT polarizability method and the RT-ESGM are compared for different functionals and basis sets and discussed in relation to Jensen's PT-TDDFT polarizability method. At last, the calculation of a full Raman excitation profile of R-methyloxirane is presented.

A. Convergence of the Padé approximation

In order to assess the performance of the Padé approximants, the absorption spectrum of uracil was calculated using the standard FFT algorithm with maximal signal length and compared to Padé approximants taking different lengths of the signal into account for determining the coefficients in Eq. (35). To measure the convergence of the Padé approximants, the root mean square of the differences between the FFT and the Padé approximants spectra was calculated at the points where the FFT is defined and normalized by the number of these points. This procedure was carried out for different time steps and the number of steps: 0.02 a.u. (500 000 steps), 0.05 a.u. (300 000 steps), and 0.10 a.u. (150 000 steps). The first 15 eV of the spectrum were included in the analysis. The results are shown in Fig. 2. As soon as a certain amount of the signals is taken into account for the Padé approximants, the difference between the FFT and the Padé approximants spectrum reaches a plateau, indicating that the respective absorption spectra are converged. Not surprisingly, this threshold depends more on the propagation time than on the amount of steps, at least for the time steps of 0.10 a.u. and 0.05 a.u. For a well converged absorption spectrum, up to an excitation energy of 15 eV, a simulation time of ~8000 a.u. (≈200 fs) is necessary for an RTP step of 0.10 a.u.

However, for the calculation of Raman spectra the excitation frequency was tuned to one of the first excitations visible in the absorption spectrum, which are usually below 10 eV. In that case, an insignificant error of ~1% was found for the resulting Raman intensities between using either ~50 fs or ~100 fs of the signal for the calculation of the Padé approximants for an RTP time step of 0.05 a.u.

Additionally, the precision for the calculation of excitation energies with Padé approximants was evaluated as follows: One excitation energy was calculated for a time step of 0.10 a.u. in the RTP and a maximal signal length of 50 000 steps.

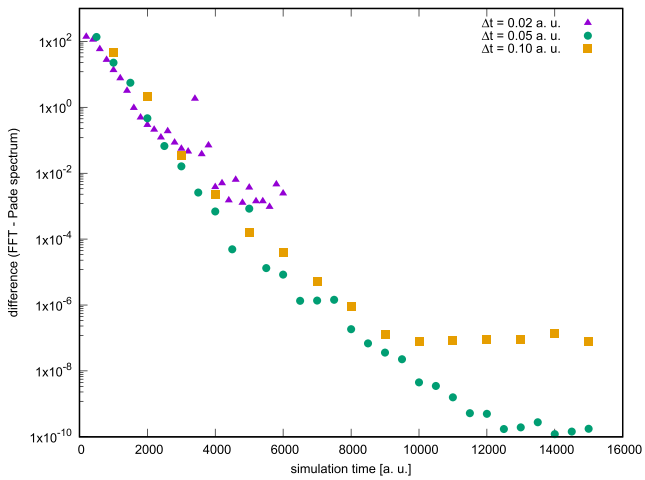

FIG. 2. Convergence of Padé approximants toward the FFT spectrum for different time steps in the RTP. On the y-axis, the root mean square between the FFT and the Padé approximants spectra is given.

Then the difference to this final value at full signal length was calculated while taking different lengths of the signal into account for determining the coefficients in Eq. (35). The result is shown in Fig. 3. The resulting excitation energy is well converged after ~3000 a.u. of simulation time with a time step of 0.10 a.u.

B. Absorption spectra

Absorption spectra of uracil and R-methyloxirane were calculated using RT-TDDFT in CP2K and PT-TDDFT in Turbomole.

For uracil, the BP86 exchange–correlation functional was used with Ahlrichs' TZVP basis set for both methods in order to be consistent with the work of Jensen[39] *et al.* on uracil. The resulting spectra are shown in Fig. 4. The RT-TDDFT spectrum is calculated according to Eq. (30) and is naturally broadened due to the damping factor Γ, whereas the PT-TDDFT spectrum is given in terms of excitation energies and corresponding oscillator strengths. Both methods agree perfectly as expected from the discussion in Sec. II since they are basically given by the same response in the case of a weak δ-pulse perturbation for the calculation of the RT-polarizability. This is consistent with the literature.[5] Also note that the RT-TDDFT spectrum extends itself to give the full spectrum from one simulation run, while the PT-TDDFT spectrum is limited to a certain energy range.

In Fig. 5, the RT-TDDFT and PT-TDDFT absorption spectra for R-methyloxirane are shown. Here the PBE functional was used with Ahlrichs' TZVP basis set. Again, both methods agree well.

C. Non-resonant Raman spectra

Non-resonance Raman (NR) spectra of R-methyloxirane were calculated with the RT polarizability method in CP2K and PT-TDDFT in Turbomole. The PT-TDDFT NR spectrum is shown in Fig. 6 for the PBE exchange–correlation functional with Ahlrichs' TZVP basis set. RTP runs were carried out for the PBE exchange–correlation functional with the TZV2P-GTH and aug-QZV2P-GTH basis sets, respectively, and for the hybrid exchange–correlation functional PBE0 with the TZV2P-GTH basis set. The resulting NR spectra at an excitation wavelength of 633 nm are shown in Fig. 7.

The normal mode frequencies differ slightly between different exchange–correlation functionals and basis sets, which is especially pronounced in the case of the hybrid exchange–correlation functional PBE0, where they are shifted up to ~50 cm^{-1} to higher wavenumbers. The relative and absolute intensities agree well across different exchange–correlation functionals and basis sets. The RT NR spectra in Fig. 7 also compare very well to the PT-TDDFT NR spectrum in Fig. 6, showing only a small difference in absolute intensities.

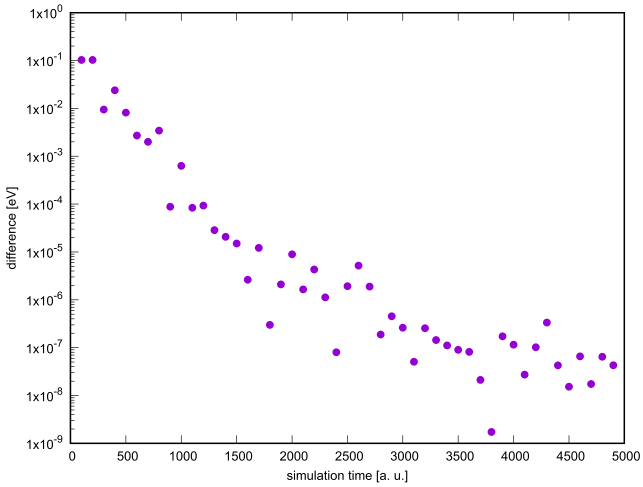

FIG. 3. Difference between the excitation energy predicted by the Padé approximants using the total signal and less for an RTP time step of 0.10 a.u. (for details see text).

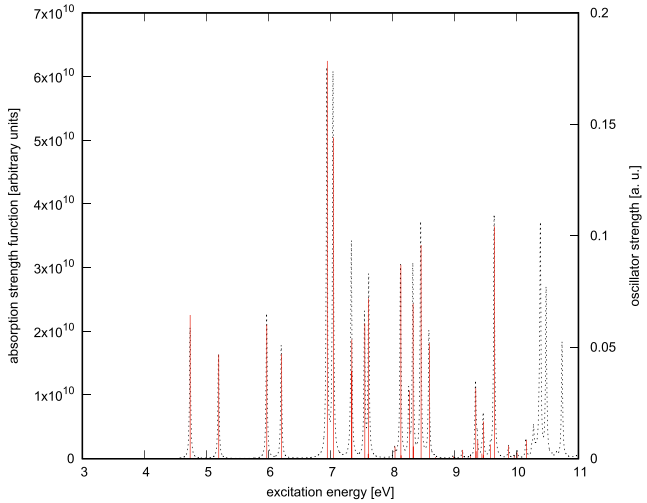

FIG. 4. Absorption spectrum of uracil calculated with PT-TDDFT (Turbomole, solid red) and RT-TDDFT (CP2K, dashed black). The BP86 exchange–correlation functional was used with Ahlrichs' TZVP basis set. The damping factor Γ was set to 0.01 eV in order to have more pronounced peaks in the RT absorption spectrum.

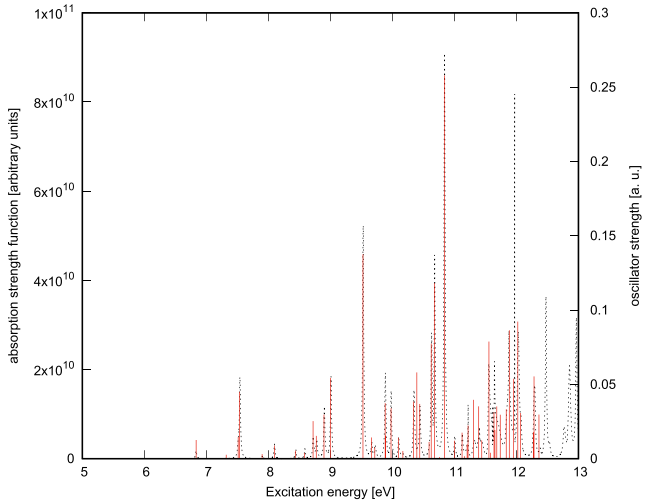

FIG. 5. Absorption spectrum of R-methyloxirane calculated with PT-TDDFT (Turbomole, solid red) and RT-TDDFT (CP2K, dashed black). The PBE exchange–correlation functional was used with Ahlrichs' TZVP basis set. The damping factor Γ was set to 0.01 eV in order to have more pronounced peaks in the RT absorption spectrum.

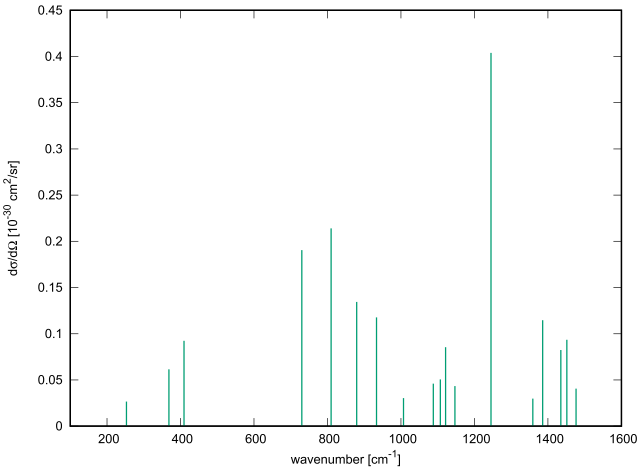

FIG. 6. Non-resonant Raman scattering cross section of R-methyloxirane for the TZVP basis set and PBE functional calculated with PT-TDDFT (Turbomole) at an excitation wavelength of 633 nm.

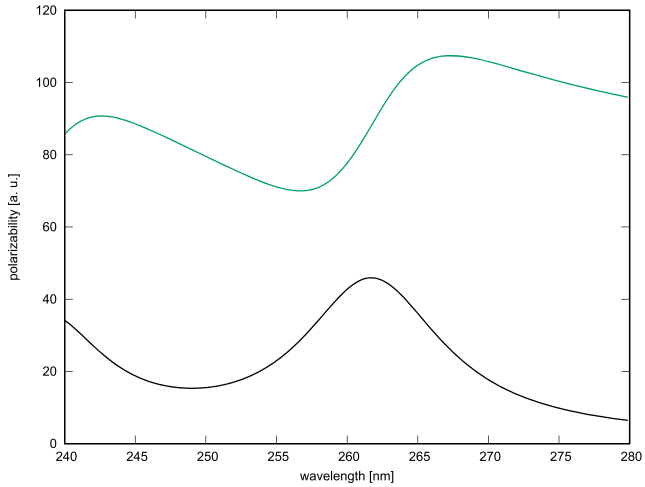

FIG. 8. Polarizability of uracil calculated with the RT polarizability method using the BP86 exchange–correlation functional with Ahlrichs' TZVP basis set. The real part is plotted in black, the imaginary part in green.

D. Resonance Raman spectra

In this section, three methods are compared for the calculation of resonance Raman (RR) spectra: The RT polarizability method described in Sec. II B 1, the RT excited state gradient method described in Sec. II C, and the PT polarizability method described in Sec. II A 2. The RT calculations were carried out by the authors, for the PT results it is referred to the work of Jensen *et al.* on uracil.[39] The presentation is split into two parts: First the RT polarizability method and the PT polarizability method are compared for uracil, then the RT polarizability method is compared to the RT excited state gradient method for R-methyloxirane.

1. Uracil—RTP and PT polarizability method

The polarizability of uracil calculated with the RT polarizability method is shown in Fig. 8. The imaginary part shows a maximum at ~263 nm (4.71 eV) consistent with the first excitation in the RT and PT absorption spectra (see Fig. 4). For the calculation of the RR spectrum, an excitation wavelength of 266 nm was chosen as well as a damping factor of 0.004 a.u. and the BP86 exchange–correlation functional with Ahlrichs' TZVP basis set, in order to be consistent with the work of Jensen *et al.*[39] The resulting RR spectrum is shown in Fig. 9.

The polarizability and consequently the RR spectrum agree perfectly with the result of Jensen *et al.* (Ref. 39, Fig. 4). Slight differences may be accounted for, among others, by the use of Gaussian type basis sets for the RT polarizability method in contrast to the Slater type basis sets used by Jensen *et al.* for the PT polarizability method. This agreement between the two methods is expected because they are essentially in accordance in the regime where perturbation theory is valid, as shown in Sec. II. Thomas *et al.* observed a good agreement between the two methods for *ortho*-nitrophenol[43] as well.

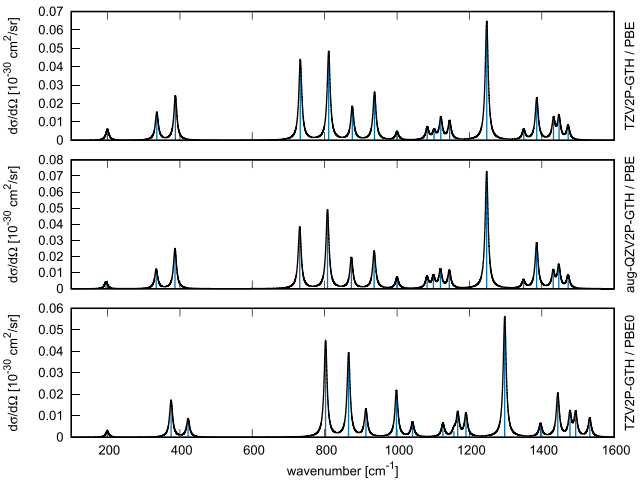

FIG. 7. Non-resonant Raman scattering cross section of R-methyloxirane calculated with the RT polarizability method at an excitation energy of 633 nm. The phenomenological damping factor Γ was set to 0.1 eV ≈ 0.0037 a.u. The Raman peaks were broadened by a Lorentzian with a full width at half maximum (FWHM) of 10 cm^{-1}.

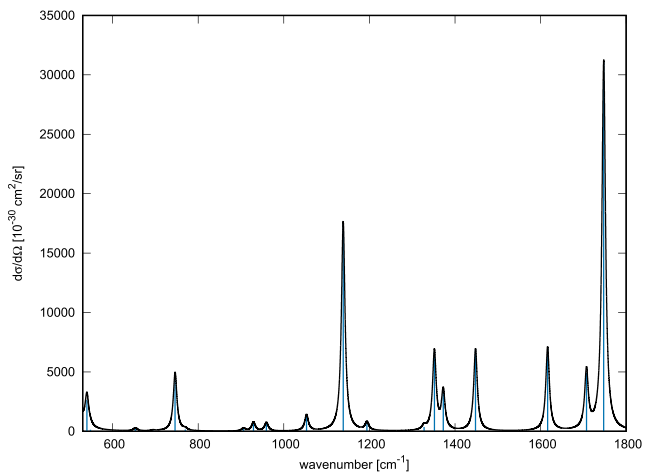

FIG. 9. RR scattering cross section of uracil calculated with the RT polarizability method using the BP86 exchange–correlation functional with Ahlrichs' TZVP basis set. The phenomenological damping factor Γ was set to 0.004 a.u. The Raman peaks were broadened by a Lorentzian with a FWHM of 10 cm^{-1}.

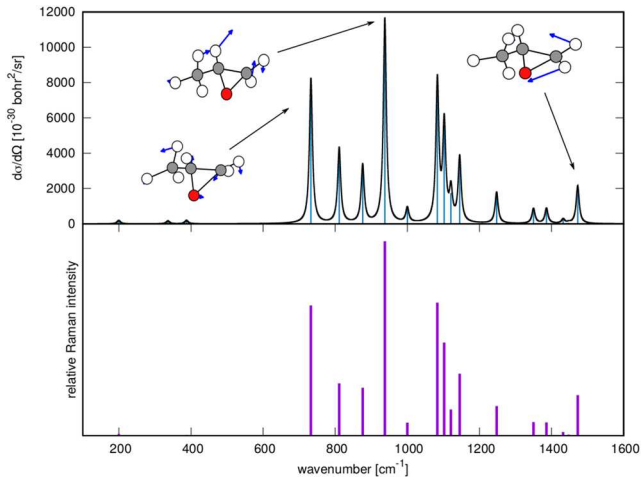

FIG. 10. RR scattering cross section of R-methyloxirane calculated with the RT polarizability method (upper) and the RT excited state gradient method (lower). The PBE exchange–correlation functional was used with the TZV2P-GTH basis set. The peaks in the RT polarizability spectrum have been broadened by a Lorentzian with a FWHM of 10 cm^{-1}. Selected normal modes are shown in the upper panel.

2. R-methyloxirane—RT polarizability and RT excited state gradient method

In this section, the RT excited state gradient method, which is enabled by using Padé approximants, is compared to the RT polarizability method for R-methyloxirane. In the following, the TZV2P-GTH basis set is used in combination with the PBE exchange–correlation functional and its hybrid version PBE0. The excitation frequency for the calculation of RR was set to the first excitation visible in the absorption spectrum, at 7.09 eV in the case of the PBE and at 7.93 eV in the case of the PBE0.

The resulting RR spectra together with pictures of selected normal modes are shown in Fig. 10 for the PBE exchange–correlation functional. There is a strong increase

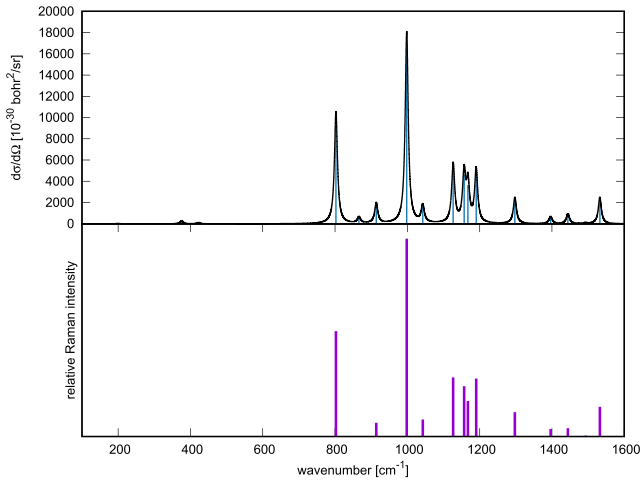

FIG. 11. RR scattering cross section of R-methyloxirane calculated with the RT polarizability method (upper) and the RT excited state gradient method (lower). The PBE0 exchange–correlation functional was used with the TZV2P-GTH basis set. The peaks in the RT polarizability spectrum have been broadened by a Lorentzian with a FWHM of 10 cm^{-1}.

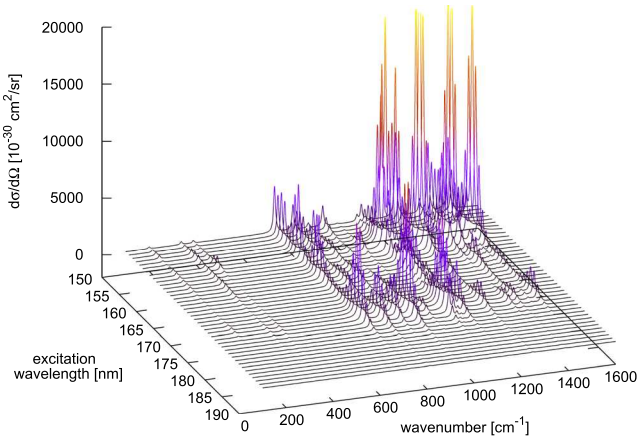

FIG. 12. Excitation profile of R-methyloxirane using PBE exchange–correlation functional and the TZV2P-GTH basis set. The resonance Raman effect is clearly visible. The Raman peaks were broadened by a Lorentzian with a FWHM of 10 cm^{-1}.

of the intensity compared to the non-resonant case (see Fig. 7) of a factor of 10^5–10^6, which is consistent with experimental results.[75]

The relative RR intensities given by the RT excited state gradient method match perfectly with the relative intensities predicted by the RT polarizability method. This is expected since both methods involve STAs to the excited state dynamics. This correspondence was also observed by Thomas *et al.*[43] and Kane and Jensen[54] who applied the excited state gradient method in a PT-TDDFT framework.

The RR spectra computed with the PBE0 hybrid exchange–correlation functional with the TZV2P-GTH basis set are shown in Fig. 11. They are comparable to the ones calculated with the PBE functional (see Fig. 10), but the relative intensities and the features between ∼1000 cm^{-1} and ∼1200 cm^{-1} show considerable differences. As noticed in the NRS case, the normal mode frequencies are shifted to higher wavenumbers.

E. Excitation profile of R-methyloxirane

The key advantage of the RT polarizability method is that the NR and RR spectra are calculated from one and the same set of simulations and the excitation frequency can be tuned to an arbitrary value by virtue of the Padé approximants. Thus the whole Raman excitation profile can be obtained in one run. This is illustrated for R-methyloxirane in Fig. 12.

V. CONCLUSION

We have presented efficient methods to calculate (resonance) Raman spectra via real-time propagation. Besides the automatic evaluation of entire excitation profiles, several short time approximations to the KHD tensor for the calculation of Raman spectra were examined: The RT polarizability method, where RTP of the time-dependent Kohn–Sham equations is used to calculate the electronic polarizability, and the excited state gradient method from Heller *et al.*[38]

Using the unified language of (linear) response theory and calculations, the RT polarizability method and the PT polarizability method from Jensen *et al.*[39] were shown to be in excellent agreement in the case of a weak δ-pulse perturbation as earlier results from Thomas *et al.*[43] suggested. This has been demonstrated for absorption and resonance Raman spectra of uracil.

The great advantage of the RT method, that the whole excitation frequency range is obtained in just one set of simulations, is illustrated by a Raman excitation profile of R-methyloxirane. With the help of Padé approximants to the FT required in an RTP framework, the excitation frequency can be tuned to an arbitrary value and the transition from non-resonant and resonance Raman spectra can be monitored in fine detail (see Fig. 12).

The convergence of Padé approximants dependent on the simulation time was evaluated for absorption spectra, and a simulation time of at most ∼5000 fs was found to be necessary for the calculation of Raman spectra at an RTP time step of 0.10 a.u. Taking further advantage of Padé approximants, the excited state gradient method has been extended to an RTP framework: Padé approximants allow us to achieve the necessary resolution in the frequency domain to perform the derivatives of excited state energies in the Condon approximation numerically, by determining the peak positions (excitation energies) in the RT absorption spectra for the displaced geometries. The formula found by Heller *et al.*[38] can then be applied directly. Subsequently this new RT excited state gradient method was compared to the RT-polarizability method for RRS spectra of R-methyloxirane and found to be in good agreement.

Additionally the NR spectra calculated with the RT polarizability method were compared with the NR spectra calculated in a PT-TDDFT framework for R-methyloxirane, and a very good agreement was found.

In summary, RTP is a promising approach to efficiently calculate Raman spectra for off- and on resonance cases also for overlapping excited states. A newly created toolbox allows now automatic evaluation of whole excitation profiles as well as the application of the excited state gradient method via RTP and the use of Padé approximants. These approaches will be very valuable for spectroscopic investigation of functional systems, in particular for light-driven catalysis such as water spitting.

ACKNOWLEDGMENTS

This work has been supported by the University of Zurich, the University Research Priority Program "Solar Light to Chemical Energy Conversion" (LightChEC), and the Swiss National Foundation (Grant No. PP00P2_170667). Our calculations have been supported by the Swiss National Supercomputing Center, Account Nos. s745 and s788.

APPENDIX A: TIME-DEPENDENT PERTURBATION THEORY

For the derivation of a time-dependent perturbation theory expression for the susceptibility [Eq. (23)], it is convenient to change the description to the interaction picture since here the unperturbed wave functions are used naturally as basis and the time evolution is shifted to the operators. Again we closely follow Ref. 55 for the presentation of the theory.

The equation of motion (e.o.m.) in the interaction picture can be written as

$$\frac{\mathrm{d}}{\mathrm{d}t}\hat{\rho}_I(t) = -\frac{i}{\hbar}e^{i\hat{H}_0 t/\hbar}\left[\hat{H}_1(t), \hat{\rho}(t)\right]e^{-i\hat{H}_0 t/\hbar}, \tag{A1}$$

where

$$\hat{\rho}_I(t) = e^{i\hat{H}_0 t/\hbar}\hat{\rho}(t)e^{-i\hat{H}_0 t/\hbar} \tag{A2}$$

is the time-dependent density operator in the interaction picture and $\hat{\rho}(t) = \hat{\rho}_0 + \hat{\rho}_1(t)$ is the time-dependent density operator split into the unperturbed part $\hat{\rho}_0$ and a time-dependent part $\hat{\rho}_1(t)$.

Since $\hat{H}_1(t)$ is linear in $f(t)$ [see Eq. (20)], one can replace $\hat{\rho}(t)$ by $\hat{\rho}_0$ in linear response; i.e., only terms linear in the perturbation strength are considered in the e.o.m.,

$$\begin{aligned}\frac{\mathrm{d}}{\mathrm{d}t}\hat{\rho}_I &\approx -\frac{i}{\hbar}e^{i\hat{H}_0 t/\hbar}\left[\hat{H}_1, \hat{\rho}_0\right]e^{-i\hat{H}_0 t/\hbar}\\ &= \frac{i}{\hbar}\left[\hat{A}_0(t), \hat{\rho}_0\right]f(t),\end{aligned} \tag{A3}$$

with

$$\hat{A}_0(t) = e^{i\hat{H}_0 t/\hbar}\hat{A}e^{-i\hat{H}_0 t/\hbar}, \tag{A4}$$

which corresponds to evolution of the perturbation operator in the Heisenberg picture of the unperturbed system. Using Eqs. (A2) and (A3), the time evolution of the density operator to first order in the perturbation can be expressed as

$$\hat{\rho}(t) = \hat{\rho}_0 + \frac{i}{\hbar}\int_{-\infty}^{t}\mathrm{d}t'\ [A_0(t'-t),\ \hat{\rho}_0]f(t'), \tag{A5}$$

allowing us to write the expectation value in Eq. (22) as

$$\begin{aligned}\langle\hat{B}(t)\rangle - \langle\hat{B}\rangle &= \mathrm{Tr}\left\{(\hat{\rho}(t) - \hat{\rho}_0)\hat{B}\right\}\\ &= \frac{i}{\hbar}\int_{-\infty}^{t}\mathrm{d}t'\left\langle\left[\hat{B},\ \hat{A}_0(t'-t)\right]\right\rangle_0 f(t').\end{aligned} \tag{A6}$$

The braket $\langle\rangle_0$ is the same as in Eq. (21), but referring to the equilibrium density ρ_0 and not $\rho(t)$. Identifying the response function from Eq. (22) with

$$\Phi_{BA}(t-t') = \frac{i}{\hbar}\theta(t-t')\left\langle\left[\hat{B}_0(t), \hat{A}_0(t')\right]\right\rangle_0 \tag{A7}$$

gives the so-called Kubo formula (θ is the Heaviside function). $\hat{B}_0(t)$ is operator $\hat{B}$ propagated in time according to Eq. (A4). A general response function can now be written as (omitting the index 0)

$$\begin{aligned}K_{BA}(t-t') &= \frac{i}{\hbar}\left\langle\left[\hat{B}(t), \hat{A}(t')\right]\right\rangle\\ &= \frac{i}{\hbar}\mathrm{Tr}\left\{\hat{\rho}_0\left[\hat{B}(t), \hat{A}(t')\right]\right\}.\end{aligned} \tag{A8}$$

APPENDIX B: REAL TIME PROPAGATION OF THE TIME-DEPENDENT KOHN–SHAM EQUATIONS

Here the RTP in a TDDFT framework which was used in this work is briefly sketched. Analogous to ground state DFT,[76] the Kohn–Sham approach[77] combined with the Runge-Gross

theorem[78] allows us to treat the time-dependent many-body Schrödinger equation (TDSE)[79] in terms of one electron functions $|\psi^i(r,\,t)\rangle$ (orbitals), which constitute the solution for a non-interacting reference system, a Slater determinant,[80] that reproduces the real electron density. The TDSE is then represented by the following form, known as the time-dependent Kohn–Sham (TDKS) equations:

$$i\frac{\partial}{\partial t}|\psi^i(r,t)\rangle = \hat{H}_{\mathrm{KS}}|\psi^i(r,t)\rangle = \left[-\frac{\Delta_r}{2} + \hat{V}_{\mathrm{eff}}(r,t)\right]|\psi^i(r,t)\rangle \tag{B1}$$

with the effective potential

$$\hat{V}_{\mathrm{eff}}(r,t) = \hat{V}_{\mathrm{ext}}(r,t) + \int \mathrm{d}r' \frac{\rho(r,t)}{|r-r'|} + \hat{V}_{\mathrm{xc}}(r,t) \tag{B2}$$

and the electron density $\rho(r,\,t)$. For simplicity, only closed shell systems are considered in the description here.

Here $\hat{V}_{\mathrm{xc}}(r,t)$ denotes the time-dependent exchange–correlation potential. In order to emulate the real electron density, it would have to be dependent on the initial state and the history of the electron density,[81] but for every day calculations usually the adiabatic approximation is invoked,[2]

$$V_{\mathrm{xc}}[\rho](r,t) = V_{\mathrm{xc}}[\rho_t](r), \tag{B3}$$

where ρ_t is the electron density at time t. On the one hand, this local approximation in time allows the use of common exchange–correlation functionals of ground state DFT, on the other hand RT-TDDFT calculations in the adiabatic approximation suffer from known issues such as peak-shifting,[82,83] non-physical time-dependent resonances,[84,85] and of course the usual errors originating from not using the exact exchange–correlation functional for ground state DFT.

For practical purposes, the orbitals $|\psi^i(r,\,t)\rangle$ can be expanded into a set of atom-centered (R_A denotes the position of atom A) basis functions (linear combination of atomic orbitals ansatz) with time-dependent coefficients $a_j^i(t)$

$$|\psi^i(r,t)\rangle = \sum_j a_j^i(t)\phi_j^A(r-R_A), \tag{B4}$$

which allows us to cast the TDKS (B1) into its basis representation,[86]

$$\dot{a} = -iS^{-1}\hat{H}_{\mathrm{KS}}a, \tag{B5}$$

with $a = (a_1, \ldots, a_{N_{bf}})$, where N_{bf} is the total number of basis functions, $\hat{H}_{\mathrm{KS}}$ is the Kohn-Sham Hamiltonian matrix with elements $\langle\phi_j|\hat{H}_{\mathrm{KS}}|\phi_k\rangle$ (in the atomic orbital representation), and S is the overlap matrix with elements $\langle\phi_i\phi_k\rangle$.

Equation (B5) can now be integrated numerically by using approximate propagators for short time steps

$$a(t+\Delta t) = U(t+\Delta t, t)a(t). \tag{B6}$$

There exist various choices for the propagator $U(t+\Delta t,\,t)$,[87] e.g., enforced time reversal symmetry

$$U(t+\Delta t) = e^{-\Delta t/2X(t+\Delta t)}e^{-\Delta t/2X(t)}, \tag{B7}$$

$$X(t) = iS^{-1}\hat{H}_{\mathrm{KS}}(t). \tag{B8}$$

The errors induced by the RTP scheme itself are twofold:[4] First, the propagator (i.e., the Hamiltonian) depends on time and the electron density has to be interpolated for Δt. It has been suggested to do this self consistently,[87] but there is an ongoing debate whether the additional computational cost is worth the gained precision of the calculation.[88] Second, for the reasonably sized system the matrix exponentials necessary for the propagation have to be approximated as well.[89,90] Usually this is done by series expansions, subspace algorithms, or splitting techniques.

[1] R. M. Sternheimer, Phys. Rev. **96**, 951 (1954).
[2] M. E. Casida, *Recent Advances in Computational Chemistry* (World Scientific, 1995), Vol. 1, pp. 155–192.
[3] J. J. Goings, P. J. Lestrange, and X. Li, Wiley Interdiscip. Rev.: Comput. Mol. Sci. **8**, e1341 (2017).
[4] M. R. Provorse and C. M. Isborn, Int. J. Quantum Chem. **116**, 739 (2016).
[5] S. Tussupbayev, N. Govind, K. Lopata, and C. J. Cramer, J. Chem. Theory Comput. **11**, 1102 (2015).
[6] M. A. L. Marques and A. Rubio, in *Time-Dependent Density Functional Theory*, edited by M. Marques, C. A. Ullrich, F. Nogueira, A. Rubio, K. Burke, and E. K. Gross (Springer-Verlag, Berlin, Heidelberg, 2006), Chap. 15, pp. 227–240.
[7] S. Andermatt, J. Cha, F. Schiffmann, and J. VandeVondele, J. Chem. Theory Comput. **12**, 3214 (2016).
[8] S. Tretiak and V. Chernyak, J. Chem. Phys. **119**, 8809 (2003).
[9] Y. Takimoto, F. D. Vila, and J. J. Rehr, J. Chem. Phys. **127**, 154114 (2007).
[10] K. Yabana and G. F. Bertsch, Int. J. Quantum Chem. **75**, 55 (1999).
[11] F. Ding, B. E. Van Kuiken, B. E. Eichinger, and X. Li, J. Chem. Phys. **138**, 064104 (2013).
[12] J. J. Goings and X. Li, J. Chem. Phys. **144**, 234102 (2016).
[13] K.-M. Lee, K. Yabana, and G. F. Bertsch, J. Chem. Phys. **134**, 144106 (2011).
[14] C. L. Cheng, J. S. Evans, and T. Van Voorhis, Phys. Rev. B **74**, 155112 (2006).
[15] A. Petrone, D. B. Lingerfelt, N. Rega, and X. Li, Phys. Chem. Chem. Phys. **16**, 24457 (2014).
[16] M. Kadek, L. Konecny, B. Gao, M. Repisky, and K. Ruud, Phys. Chem. Chem. Phys. **17**, 22566 (2015).
[17] M. Repisky, L. Konecny, M. Kadek, S. Komorovsky, O. L. Malkin, V. G. Malkin, and K. Ruud, J. Chem. Theory Comput. **11**, 980 (2015).
[18] U. De Giovannini, G. Brunetto, A. Castro, J. Walkenhorst, and A. Rubio, ChemPhysChem **14**, 1363 (2013).
[19] D. Cho, J. R. Rouxel, M. Kowalewski, P. Saurabh, J. Y. Lee, and S. Mukamel, J. Phys. Chem. Lett. **9**, 1072 (2018).
[20] D. P. Strommen and K. Nakamoto, J. Chem. Educ. **54**, 474 (1977).
[21] S. Hu, K. M. Smith, and T. G. Spiro, J. Am. Chem. Soc. **118**, 12638 (1996).
[22] T. Nagasao and P. D. Mitchell, J. Raman Spectrosc. **3**, 153 (1975).
[23] Z. Ni, Y. Wang, T. Yu, Y. You, and Z. Shen, Phys. Rev. B **77**, 235403 (2008).
[24] A. Jorio, M. A. Pimenta, A. G. S. Filho, R. Saito, G. Dresselhaus, and M. S. Dresselhaus, New J. Phys. **5**, 139 (2003).
[25] B. W. Park, S. M. Jain, X. Zhang, A. Hagfeldt, G. Boschloo, and T. Edvinsson, ACS Nano **9**, 2088 (2015).
[26] C. Li, T. Ahmed, M. Ma, T. Edvinsson, and J. Zhu, Appl. Catal., B **138-139**, 175 (2013).
[27] D. Friebel, M. W. Louie, M. Bajdich, K. E. Sanwald, Y. Cai, A. M. Wise, M. J. Cheng, D. Sokaras, T. C. Weng, R. Alonso-Mori, R. C. Davis, J. R. Bargar, J. K. Nørskov, A. Nilsson, and A. T. Bell, J. Am. Chem. Soc. **137**, 1305 (2015).
[28] L. Jensen, J. Autschbach, M. Krykunov, and G. C. Schatz, J. Chem. Phys. **127**, 134101 (2007).
[29] S. Luber, J. Neugebauer, and M. Reiher, J. Chem. Phys. **132**, 044113 (2010).
[30] S. Luber and M. Reiher, ChemPhysChem **11**, 1876 (2010).
[31] H. A. Kramers and W. Heisenberg, Z. Phys. A: Hadrons Nucl. **31**, 681 (1925).
[32] P. A. M. Dirac, Proc. R. Soc. London, Ser. A **114**, 710 (1927).
[33] A. C. Albrecht, J. Chem. Phys. **34**, 1476 (1961).
[34] G. Herzberg and E. Teller, Z. Phys. Chem. **21B**, 410 (1933).
[35] J. Guthmuller and B. Champagne, J. Chem. Phys. **127**, 164507 (2007).
[36] S. Lee, J. Chem. Phys. **78**, 723 (1983).
[37] S.-Y. Lee and E. J. Heller, J. Chem. Phys. **71**, 4777 (1979).

[38]E. J. Heller, R. L. Sundberg, and D. Tannor, J. Phys. Chem. **86**, 1822 (1982).
[39]L. Jensen, L. L. Zhao, J. Autschbach, and G. C. Schatz, J. Chem. Phys. **123**, 174110 (2005).
[40]G. Placzek, Z. Phys. **70**, 84 (1931).
[41]H. Chen, J. M. Mcmahon, M. A. Ratner, and G. C. Schatz, J. Phys. Chem. C **114**, 14384 (2010).
[42]M. Thomas, S. Mühlig, T. Deckert-Gaudig, C. Rockstuhl, V. Deckert, and P. Marquetand, J. Raman Spectrosc. **44**, 1497 (2013).
[43]M. Thomas, F. Latorre, and P. Marquetand, J. Chem. Phys. **138**, 044101 (2013).
[44]J. Guthmuller, J. Chem. Theory Comput. **7**, 1082 (2011).
[45]A. Bruner, D. Lamaster, and K. Lopata, J. Chem. Theory Comput. **12**, 3741 (2016).
[46]D. A. Long, *The Raman Effect: A Unified Treatment of the Theory of Raman Scattering by Molecules* (John Wiley & Sons Ltd, 2002).
[47]D. J. Tannor, *Introduction to Quantum Mechanics: A Time-Dependent Perspective* (University science books, Mill Valley, CA, 2007).
[48]D. J. Tannor and E. J. Heller, J. Chem. Phys. **77**, 202 (1982).
[49]J. H. Van Vleck, Proc. Natl. Acad. Sci. U. S. A. **15**, 754 (1929).
[50]J. Neugebauer, M. Reiher, C. Kind, and B. A. Hess, J. Comput. Chem. **23**, 895 (2002).
[51]M. Reiher, J. Neugebauer, and B. A. Hess, Z. Phys. Chem. **217**, 91 (2003).
[52]T. Weymuth, M. P. Haag, K. Kiewisch, S. Luber, S. Schenk, C. R. Jacob, C. Herrmann, J. Neugebauer, and M. Reiher, J. Comput. Chem. **33**, 2186 (2012).
[53]A. Warshel and P. Dauber, J. Chem. Phys. **66**, 5477 (1977).
[54]K. A. Kane and L. Jensen, J. Phys. Chem. C **114**, 5540 (2010).
[55]J. Jensen and A. R. Mackintosh, *Rare Earth Magnetism: Structures and Excitations* (Clarendon Press, Oxford, 1991), pp. 134–162.
[56]G. Frobenius, J. Reine Angew. Math. **1881**(90), 1.
[57]H. Padé, Ann. Sci. l'École Norm. Supérieure **9**, 3 (1892).
[58]J. Hutter, M. Iannuzzi, F. Schiffmann, and J. Vandevondele, Wiley Interdiscip. Rev.: Comput. Mol. Sci. **4**, 15 (2014).
[59]CP2K version 6.0 (Developement version), the CP2K developers group (2017), available from http://www.cp2k.org.
[60]S. Goedecker and M. Teter, Phys. Rev. B **54**, 1703 (1996).
[61]F. Weigend and R. Ahlrichs, Phys. Chem. Chem. Phys. **7**, 3297 (2005).
[62]J. Hutter, M. Parrinello, and G. Lippert, Theor. Chem. Acc. **103**, 124 (1999).
[63]J. Vandevondele, M. Krack, F. Mohamed, M. Parrinello, T. Chassaing, and J. Hutter, Comput. Phys. Commun. **167**, 103 (2005).
[64]J. P. Perdew, K. Burke, and M. Ernzerhof, Phys. Rev. Lett. **77**, 3865 (1996).
[65]J. P. Perdew, M. Ernzerhof, and K. Burke, J. Chem. Phys. **105**, 9982 (1996).
[66]C. Adamo and V. Barone, J. Chem. Phys. **110**, 6158 (1999).
[67]J. P. Perdew, Phys. Rev. B **33**, 8822 (1986).
[68]A. D. Becke, Phys. Rev. A **38**, 3098 (1988).
[69]W. G. Bickley, Math. Gaz. **25**, 19 (1941).
[70]K. Yabana, T. Nakatsukasa, J. I. Iwata, and G. F. Bertsch, Phys. Status Solidi B **243**, 1121 (2006).
[71]J. Kiefer, Proc. Am. Math. Soc. **4**, 502 (1953).
[72]TURBOMOLE V7.2 2017, a development of University of Karlsruhe and Forschungszentrum Karlsruhe GmbH, 1989-2007, TURBOMOLE GmbH, since 2007, available from http://www.turbomole.com.
[73]D. Rappoport and F. Furche, J. Chem. Phys. **126**, 201104 (2007).
[74]F. Furche, R. Ahlrichs, C. Hättig, W. Klopper, M. Sierka, and F. Weigend, Wiley Interdiscip. Rev.: Comput. Mol. Sci. **4**, 91 (2014).
[75]S. A. Asher, Annu. Rev. Phys. Chem. **39**, 537 (1988).
[76]P. Hohenberg and W. Kohn, Phys. Rev. **136**, B864 (1964).
[77]W. Kohn and L. J. Sham, Phys. Rev. **140**, A1133 (1965).
[78]E. Runge and E. K. U. Gross, Phys. Rev. Lett. **52**, 997 (1984).
[79]E. Schrödinger, Phys. Rev. **28**, 1049 (1926).
[80]J. C. Slater, Phys. Rev. **34**, 1293 (1929).
[81]N. T. Maitra, K. Burke, and C. Woodward, Phys. Rev. Lett. **89**, 023002 (2002).
[82]J. I. Fuks, K. Luo, E. D. Sandoval, and N. T. Maitra, Phys. Rev. Lett. **114**, 183002 (2015).
[83]M. R. Provorse, B. F. Habenicht, and C. M. Isborn, J. Chem. Theory Comput. **11**, 4791 (2015).
[84]S. Raghunathan and M. Nest, J. Chem. Theory Comput. **8**, 806 (2012).
[85]S. Raghunathan and M. Nest, J. Chem. Phys. **136**, 064104 (2012).
[86]T. Kunert and R. Schmidt, Eur. Phys. J. D **25**, 15 (2003).
[87]A. Castro and M. A. L. Marques, J. Chem. Phys. **121**, 3425 (2004).
[88]C. O'Rourke and D. R. Bowler, J. Chem. Phys. **143**, 102801 (2015).
[89]C. Moler and C. Van Loan, SIAM Rev. **45**, 3 (2003).
[90]D. Williams-Young, J. J. Goings, and X. Li, J. Chem. Theory Comput. **12**, 5333 (2016).